scientific reports

Check for updates

OPEN

A mouse model of deep vein thrombosis by inferior vena cava hypoperfusion using ameroid constrictors

Hiroko Tadokoro[1,2,3], Yukihide Ota[1,4], Mari Uomoto[1,4], Shiro Koizume[1,2], Shinya Sato[1,2,5], Yoshiyasu Nakamura[1,5], Mitsuyo Yoshihara[5,6], Yoko Endo-Takahashi[3], Yoichi Negishi[3], Etsuko Miyagi[4] & Yohei Miyagi[1,2]✉

Traditional mouse models for deep vein thrombosis (DVT), frequently utilized in research focused on cancer-associated thrombosis (CAT), reliably induce thrombus formation by obstructing blood flow (BF) in the inferior vena cava (IVC), which does not occur in humans. Therefore, to develop a new DVT model for CAT studies, we implanted an ameroid constrictor (AC), a hygroscopic casein C-shape device, around the IVC and aorta of immunocompromised mice. We evaluated the thrombus 3 and 8 days post-AC implantation and compared it with the traditional model 2 days post-vena cava ligation. The size of each thrombus was measured, and the composition was assessed using histological staining; BF through the IVC was confirmed using ultrasound imaging. The thrombus size variability in the AC and ligation models was equivalent. Compared with thrombi on day 3 post-AC implantation, those on day 8 showed characteristics of human thrombi in the subacute to chronic stage. The BF in the IVC was maintained even on day 8. In summary, the AC model showed reproducibility with no significant difference in thrombus size variability from the traditional ligation model while maintaining the BF of the IVC.

Keywords Animal model, Nude mice, Blood flow, Cancer-associated thrombosis, Venous thrombosis, Ultrasound image

Cancer-associated thrombosis (CAT) impacts the survival rate of cancer patients, and the incidence of venous thromboembolism (VTE) is increasing despite significant improvements in cancer treatment. The risk of VTE is influenced by cancer type, individual patients, and cancer treatment factors[1]. Several epidemiological studies have investigated CAT; however, data regarding the safety and efficacy of direct oral anticoagulants remain lacking[2]. The pathophysiology of CAT is complex and requires optimal animal models[1].

The most common deep vein thrombosis (DVT) models are immune-competent conventional mice, involving models ligating the inferior vena cava (IVC) (hereafter the IVC-L model)[3]or those stenosing the IVC (hereafter the IVC-S model)[4,5]. The IVC-L model obtains a highly reproducible thrombus[6,7]but terminates blood flow (BF)[6], may not precisely reflect the pathophysiology of non-trauma-related human venous thrombosis, which develops with persistent BF[8]. Therefore, due to the complete shutdown of BF in this model, evaluating the effectiveness of systemically administered anticoagulants and antiplatelet agents may not be suitable. The IVC-S model ties the IVC together with a fine needle, followed by immediate removal after ligation, resulting in approximately 90% stenosis[4,5].The IVC-S model is without obvious vascular injury[9], consistent with developing human DVT on intact vascular endothelium[10]. The thrombus formed in this model maintains the histological

[1]Molecular Pathology and Genetics Division, Kanagawa Cancer Center Research Institute, 2-3-2 Nakao, Asahi-ku, Yokohama 241-8515, Kanagawa, Japan. [2]Department of Pathology, Kanagawa Cancer Center Hospital, 2-3-2 Nakao, Asahi-ku, Yokohama 241- 8515, Kanagawa, Japan. [3]Department of Drug Delivery and Molecular Biopharmaceutics, Tokyo University of Pharmacy and Life Sciences, 1432-1 Horinouchi, Hachioji 192-0392, Tokyo, Japan. [4]Department of Obstetrics and Gynecology, Yokohama City University Graduate School of Medicine, 3-9 Fukuura, Kanazawa-ku, Yokohama 236-0004, Kanagawa, Japan. [5]Morphological Information Analysis Laboratory, Kanagawa Cancer Center Research Institute, 2-3-2 Nakao, Asahi-ku, Yokohama, Kanagawa, 241-8515, Japan. [6]Division of Advanced Cancer Therapeutics, Kanagawa Cancer Center Research Institute, 2-3-2 Nakao, Asahi-ku, , Yokohama 241-8515, Kanagawa, Japan. ✉email: miyagi.0e82r@kanagawa-pho.jp

characteristics of a human venous thrombus[9]; however, the large variability in thrombus size remains a disadvantage of this model[6,9,11]. These traditional models of DVT are currently used in studies with each associated disadvantage[5,11,12].

In both models, termination of collateral branches draining into the IVC around the area of ligation or stenosis, for example, by cauterization, significantly affects the success/failure of thrombus formation[6,13]. Although prior knowledge of anatomy and the frequency of these IVC branches are valuable for the models, they differ individually and are restricted by mouse strains[7]. Therefore, we aimed to develop a DVT model in immunocompromised nude mice that reproduces thrombogenesis and mimics the pathophysiology of human DVT to investigate the mechanisms, prophylaxis, and treatment of CAT.

An ameroid constrictor (AC) is a C-shaped ring composed of casein. Hygroscopic casein swells in ambient moisture, narrowing the luminal space of the constrictor. Mouse models using an AC as a vascular occlusion device have been developed for subcortical infarction with dementia[14]or acute hindlimb ischemia, mimicking peripheral arterial disease[15]. Although these models aim to constrict arteries, we hypothesized that implanting an AC around the mouse IVC and the descending aorta could create a novel DVT model that better mimics human diseases than the present models.

Results

Variability in thrombi obtained by the IVC hypoperfusion (IVC-H) model compared to the IVC-L model

The IVC-H and IVC-L models followed the same procedure until the cauterization of the branches of the IVC, including the right ovarian vein (Fig. 1A, B). In the IVC-L model, the IVC and aorta were locally separated to thread a suture, followed by ligation of the IVC (Fig. 1C and Supplementary Data 1–2). In contrast, in the IVC-H model, the IVC and aorta were placed together in the AC lumen (Fig. 1D and Supplementary Data 3–4).

Since the entrance occlusion of AC requires 1 day (Fig. 1E), the variability of thrombus size on the AC model on day 3 was compared with that on the ligation model on day 2. In both models, the thrombi were observed just periphery to the ligation site or the AC placement site in IVC (Fig. 2A). The thrombi obtained from the models shared the common gross characteristics of mixed thrombi with red and white stripes (Fig. 2A). The thrombi obtained from the IVC-L model were significantly larger than those obtained from the IVC-H models of the AC-8 W-3D group in weight, length, width, and mass (Fig. 2B–E).

The thrombus variability of each factor in the IVC-H (AC-8 W-3D) group was not significantly different from that of the IVC-L (Fig. 2B–E; *F*-test: $p=0.083$ for weight, $p=0.959$ for length, $p=0.139$ for width, $p=0.881$ for mass). To examine the effect of AC implantation on the variability of thrombus formation over time, we compared the thrombi derived from AC-8 W-3D and AC-8 W-8D and observed no significant difference (Fig. 2F–I). This trend was similar when using mice aged 15 weeks (Fig. S2).

Effect of processing the IVC branches in the IVC-H model

We evaluated the influence of the IVC branch processing on thrombogenesis reproducibility in the IVC-H model. First, we evaluated the number of IVC branches in the surgical procedure area in the 52 BALB/c-nu/nu mice used in the study. The numbers spanned between 0 and 4 per mouse. Mice with two branches were the most frequent, followed by those with one branch (Fig. 3A, B). Most IVC branches extended posteriorly; however, laterally extended branches were identified in three mice (Fig. 3C).

Second, we determined how the processing procedure of the IVC branches affected thrombus size. In one mouse in the AC-15 W-3D group, the thrombus terminated at the IVC branch, which was left unprocessed as it was anatomically difficult to locate (Fig. 3D). In another mouse in the same group, a small thrombus formed, and an unprocessed IVC branch was observed immediately below the AC (Fig. 3E, F).

Luminal space of the AC and actual narrowing of the IVC in the IVC-H model

We first evaluated the luminal space of the implanted AC to investigate the extent of IVC stenosis in the IVC-H model. The AC was not completely closed even after 28 days (Fig. 4A) and was buried in surrounding tissues after 3 or 8 days (Fig. 4B). The open space did not differ between the AC-3D and AC-8D groups (Fig. 4C). The space of the IVC evaluated on cross-sections in the AC-8D group was, however, significantly narrower than that of the AC-3D and non-treatment groups (Fig. 4A, B). To determine whether aortic dilation causes IVC stenosis, we investigated the correlation between the IVC luminal space and the aortic wall thickness, aortic lumen area, or aortic area (Fig. S3A–L). The IVC luminal space positively correlated with the aortic wall thickness in the AC-3D group but not in the AC-8D group (Fig. S3B–D, B: $p=0.219$, C: $p=0.050$, D: $p=0.680$). No correlation was observed between the arterial lumen area and IVC area in any group (Fig. S3F–H, F: $p=0.429$, G: $p=0.412$, H: $p=0.063$). Contrary to the expectation that arterial dilation causes IVC stenosis, AC implantation altered the positive correlation between the IVC lumen and arterial area to a moderate one (Fig. S3J–L, J: $p=0.289$, K: $p=0.016$, L: $p=0.035$).

Next, we investigated whether AC implantation conversely caused aortic stenosis (Fig. S4A–C). Although the aortic wall was significantly thickened at 3 and 8 days post-AC implantation compared with the controls (Fig. S4A), the stenosis of the aortic lumen did not occur (Fig. S4B). The aortic area, i.e., the area inside the adventitia of the aorta, which may directly affect IVC, did not significantly change (Fig. S4C). To further confirm whether AC stenosis could induce aortic stenosis, we analyzed the correlation between the AC and the aortic lumen areas (Fig. S5) and observed no correlation between them.

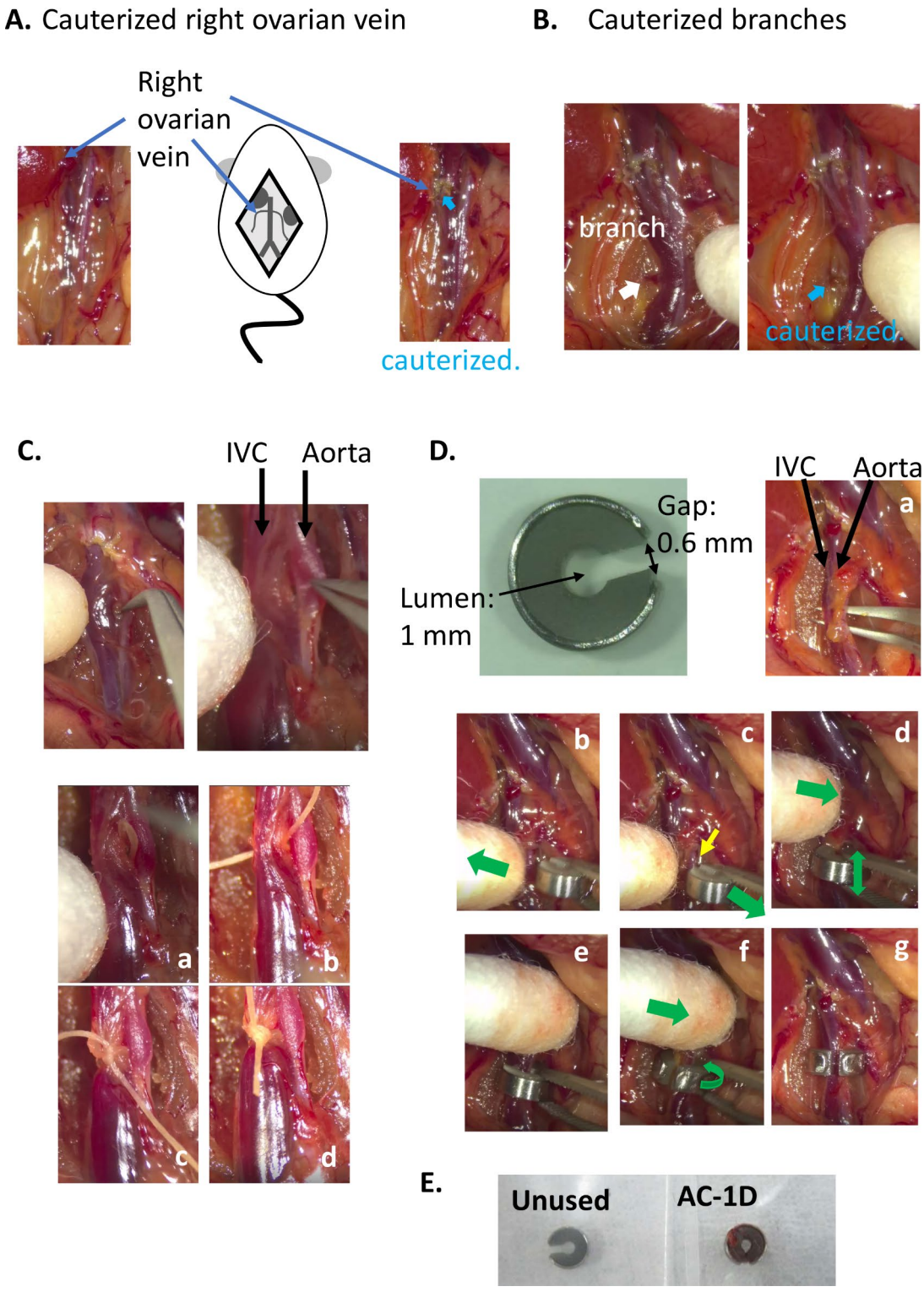

Fig. 1. Successive steps of procedures for the IVC-L and IVC-H model. (A–B) Right ovarian vein (A) and another branch of IVC (B), before (left) and after (right; light blue arrow), cauterized respectively. (C) IVC-L model. Upper two images: isolation of IVC and aorta, followed by threading between IVC and aorta (a and b) and ligation of IVC (c and d). (D) IVC-H model. Upper left panel: AC before use (left); IVC and aorta isolated *en bloc* (a). The IVC and aorta are placed into the AC lumen through the gap (b-e). The AC is finally rotated to position the gap in the front (f and g). (E) AC before use (left) and 1 day post-implantation (right). AC, ameroid constrictor; IVC, inferior vena cava; IVC-H, IVC hypoperfusion; IVC-L, IVC ligation; AC-1D, AC, one day after implantation.

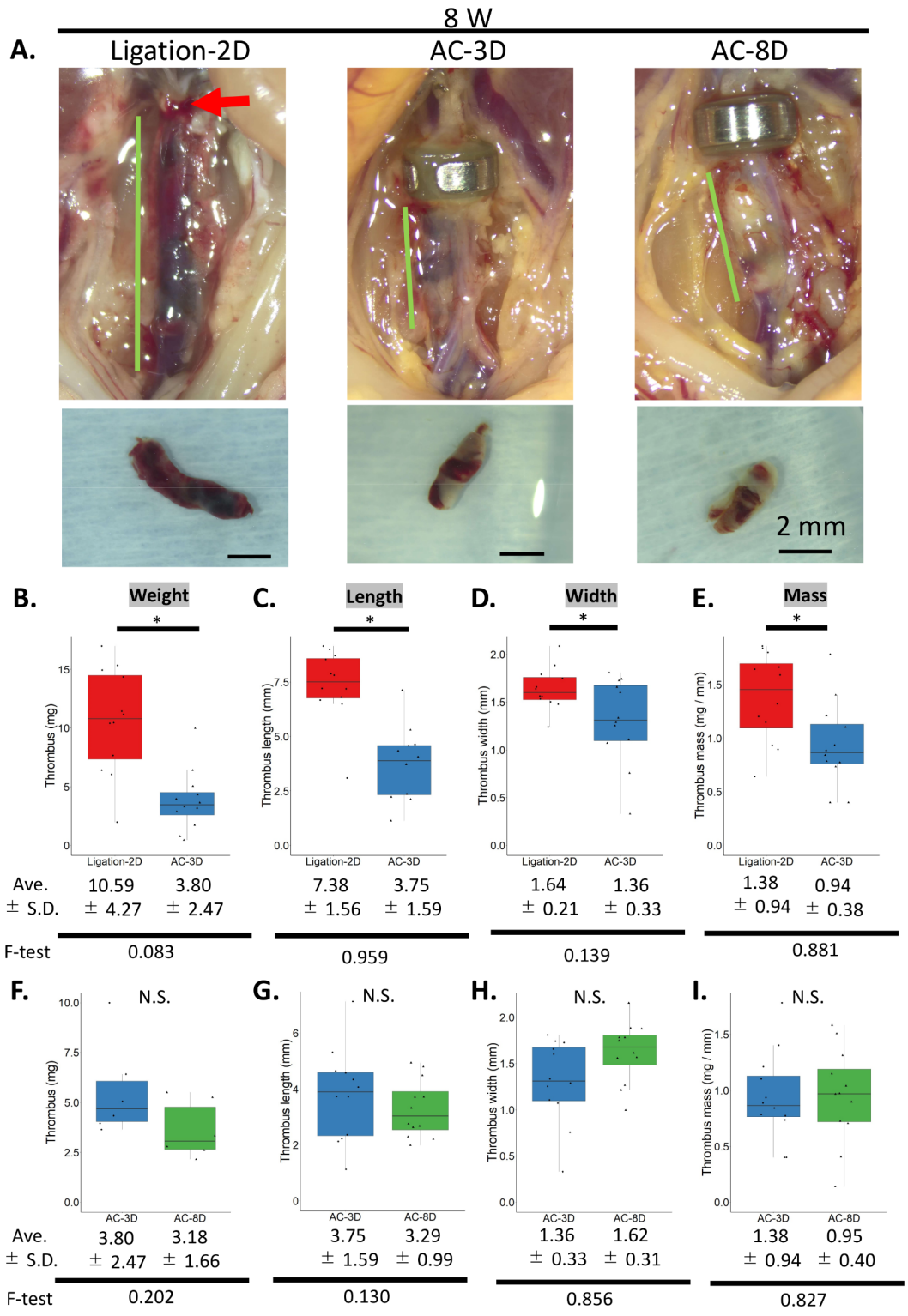

Fig. 2. Comparison of thrombi from IVC-L and IVC-H models (8-week-old mice). (A) Representative macroscopic images of thrombus in situ at day 2 (ligation-2D, left, with a red arrowhead for the ligation site) for the IVC-L model and 3 (AC-3D, middle) and 8 (AC-8D, right) for the IVC-H model. Green bars were added alongside thrombi. The black bar represents 2 mm. (B-E) Box and whisker plots of the thrombus size comparing that of ligation-2D and AC-3D (B: Weight, $*p = 1.51 \times 10^{-4}$, C: Length, $*p = 2.07 \times 10^{-5}$, D: Width (the thickest part perpendicular to the long side), $*p = 0.023$, E: Mass [weight/length], $*p = 0.014$). (F–I) Comparison of the thrombus size of AC-3D with that of AC-8D. *p*-values of the *F*-test are shown below the averages of thrombus weight (Ave) and their standard deviations (SD). $*p < 0.05$ (Student's *t*-test). AC, ameroid constrictor; IVC, inferior vena cava; IVC-H, IVC hypoperfusion; IVC-L, IVC ligation, NS: not significant.

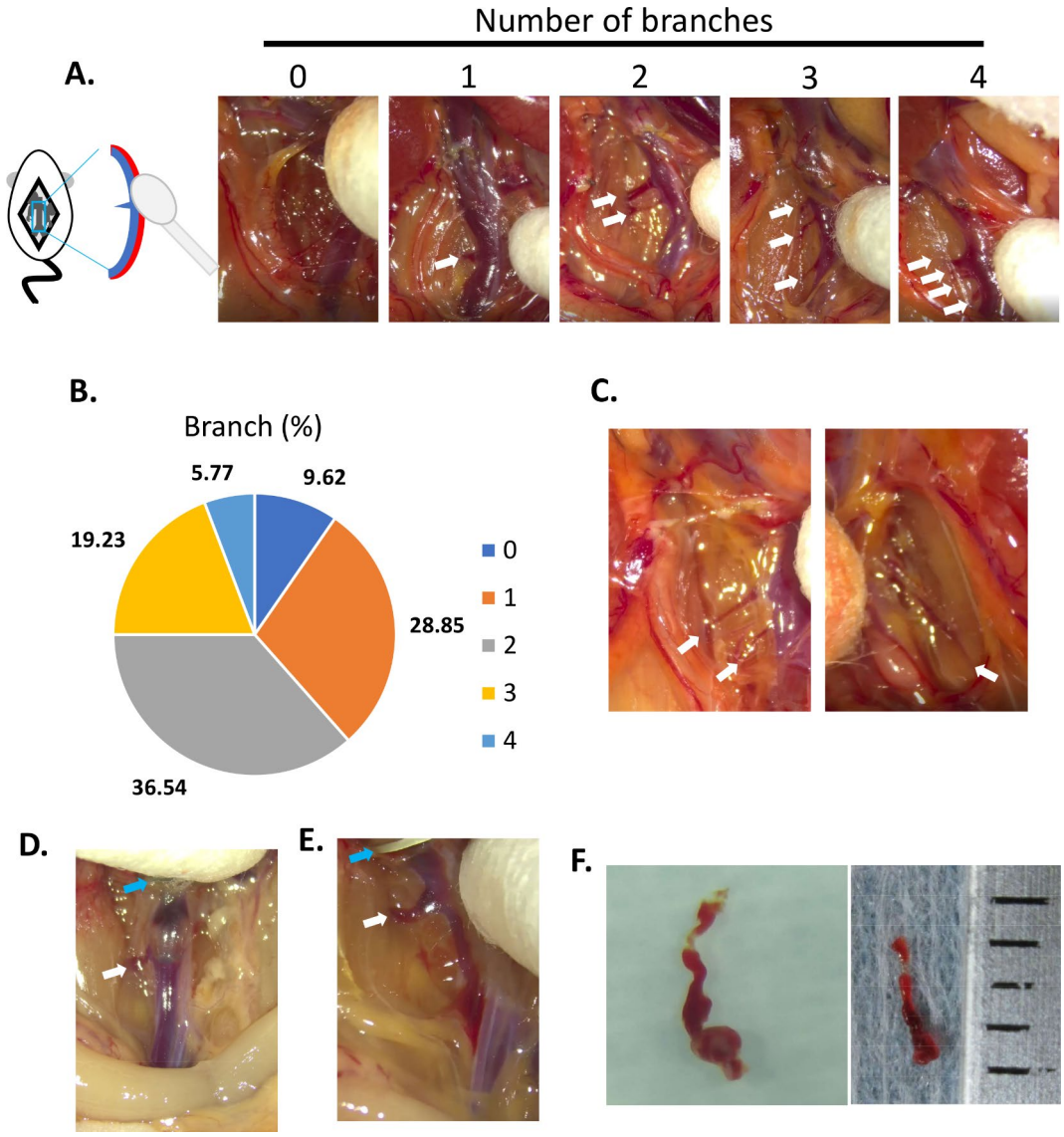

Fig. 3. Anatomical analysis of IVC branching in BALB nude (BALB/c-nu/nu) mice. (A) Representative images of branching in cases with no branch (0) to 4 branches (4) demonstrated with the tip of a cotton swab. (B) A pie chart showing the frequency of IVC branching in the field of concern in the IVC-H model among the 52 examined mice. (C) Representative images of branches entering from the lateral aspect of the IVC. (D, E) Typical images of IVC, in which directly entering branches below the AC set, were observed. Each image indicates an IVC of an individual mouse from the AC-15-3D group. (F) Insufficiently developed thrombi obtained from the IVC displayed in (E). White arrows, IVC branches; Blue arrows, AC. AC, ameroid constrictor; IVC, inferior vena cava; IVC-H, IVC hypoperfusion; IVC-L, IVC ligation.

Influence of AC implantation on BF in the IVC

Histological examinations revealed the open luminal space of the IVC even at 8 days post-AC implantation. We further evaluated the actual BF of the IVC along the course of thrombus development in the model by live imaging with an ultrasound device.

Using the image of the kidney and AC as positional references, we identified and depicted the BF of the aorta in red and of the IVC in blue, both with liquid flows shown with color bars (Fig. S6 and Supplementary Data 5 and 6). The BF of the IVC just distal to the AC was observed in multiple mice even at 8 days post-AC implantation. Mice were sacrificed after imaging to grossly assess the interpretation of ultrasound images (Fig. S6B). Since no branches entered the IVC within a 4-mm width range above the AC in this mouse, the BF identified by ultrasonography at the cranial side of the AC was the IVC's one over the AC site (Fig. S6A). The BF on the cranial side of the AC was monitored over time up to 8 days after AC implantation (Fig. 5).

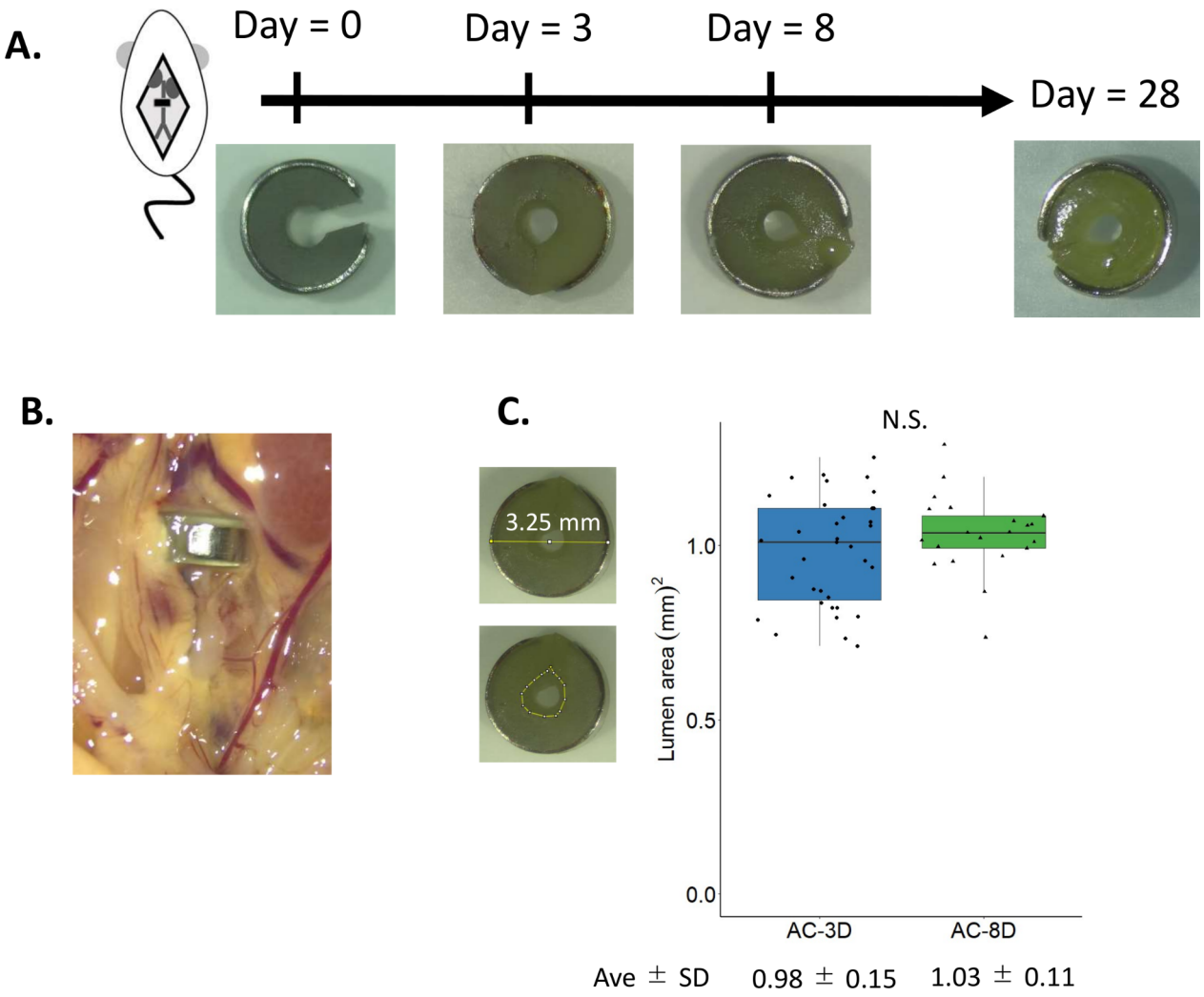

Fig. 4. Time-dependent changes in luminal space of AC placed in IVC. (A) Representative images of AC attached to IVC at the indicated time points. (B) Representative appearance of the AC just before IVC/aorta and thrombus retrieval. (C) Comparison of the open luminal area between AC implanted for 3 and 8 days (AC-3D and AC-8D). The luminal area was measured using *Image J Fiji* , which had an AC diameter of 3.25 mm as the scale and was demonstrated in box and whisker plots. Each black dot indicates an AC, AC-3D: $n = 35$; AC-8D: $n = 21$. (F -test $p = 0.142$, Student's t- test $p = 0.206$). AC, ameroid constrictor; IVC, inferior vena cava; NS, not statistically significant.

Characteristics of thrombi obtained by the IVC-H model

Thrombi obtained from the IVC-H model were histopathologically characterized. First, monocyte/macrophage areas were evaluated by Mac-2 immunohistochemistry (IHC) (Fig. 6A–C). The area was significantly larger in thrombi from the AC-8D group than those from the AC-3D group (Fig. 6C), demonstrating that the AC-8D thrombus represented a state closer to subacute to chronic venous thrombus in human diseases.

Martius Scarlet Blue (MSB) staining, cluster of differentiation (CD) 41 IHC, Col1A1 IHC for type 1 collagen alpha 1 chain, and TER119 for RBCs IHC were performed on each thrombus (Fig. 7A–J, S7A–J). The color deconvolution method applied to the MSB images showed the collagen in blue-colored and fibrin/fibrinogen (hereafter just fibrin) in red-colored areas, and red blood cells (RBCs) in yellow (Fig. 7A–J, S7A–J, S8A–I). The thrombi obtained from the AC-8 W-8D experiments showed increased collagen compared with those of the AC-8 W-3D experiments (Fig. 7E and S8B). Fibrin and RBCs were more enriched in AC-8 W-3D thrombi than those in AC-8 W-8D thrombi (Fig. 7F, G). IHC staining of collagen using Col1A1 staining showed an increased tendency in AC-8D regardless of age, although the difference was not significant (Fig. 7I). Meanwhile, IHC staining of RBCs using TER119 showed no expression change in any group (Fig. 7J). Thrombi from the IVC-L model had similar proportions of components to thrombi in the AC-3D group (Fig. S7). Platelet content evaluated with CD41 IHC was unchanged in the thrombi obtained from all experiments (Fig. 7H, S7H).

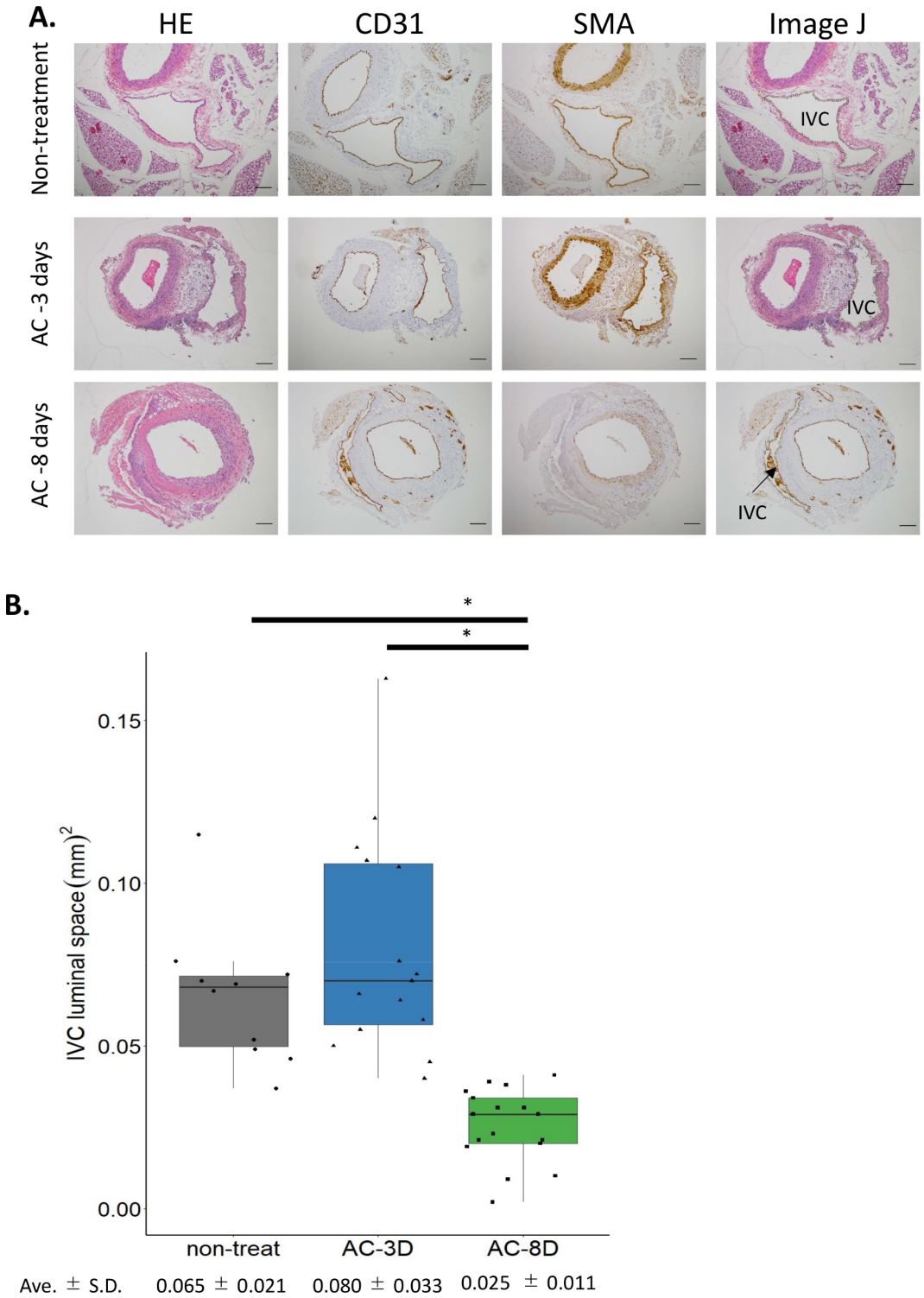

Fig. 5. IVC luminal space at different time durations following AC placement. (A) Representative histological images of IVC and aorta. Images of HE and IHC for CD31 (endothelial cells) and SMA (smooth muscle cells) for non-treatment mice and mice of the IVC-H AC-3 and AC-8 groups (non-treatment mice: 20-weeks old; IVC-H mice: 9-weeks old). Images labeled "Image J" indicate each IVC area evaluated using *Image J Fiji* . Scale bar = 100 μm. (B) Box and whisker plots comparing the IVC luminal space. Each black dot indicates an individual mouse, non-treatment: $n = 10$, AC-3D: $n = 15$, and AC-8D: $n = 17$. * $p < 0.05$ (ANOVA $p = 4.24 \times 10^{-7}$ and Tukey–Kramer; non-treat vs. AC-8D $p = 4.97 \times 10^{-4}$, AC-3D t vs. AC-8D $p = 4.00 \times 10^{-7}$). ANOVA, analysis of variance; CD, cluster of differentiation; HE, hematoxylin and eosin; IVC, inferior vena cava; IVC-H, IVC hypoperfusion; SMA, smooth muscle actin; IHC, immunohistochemistry.

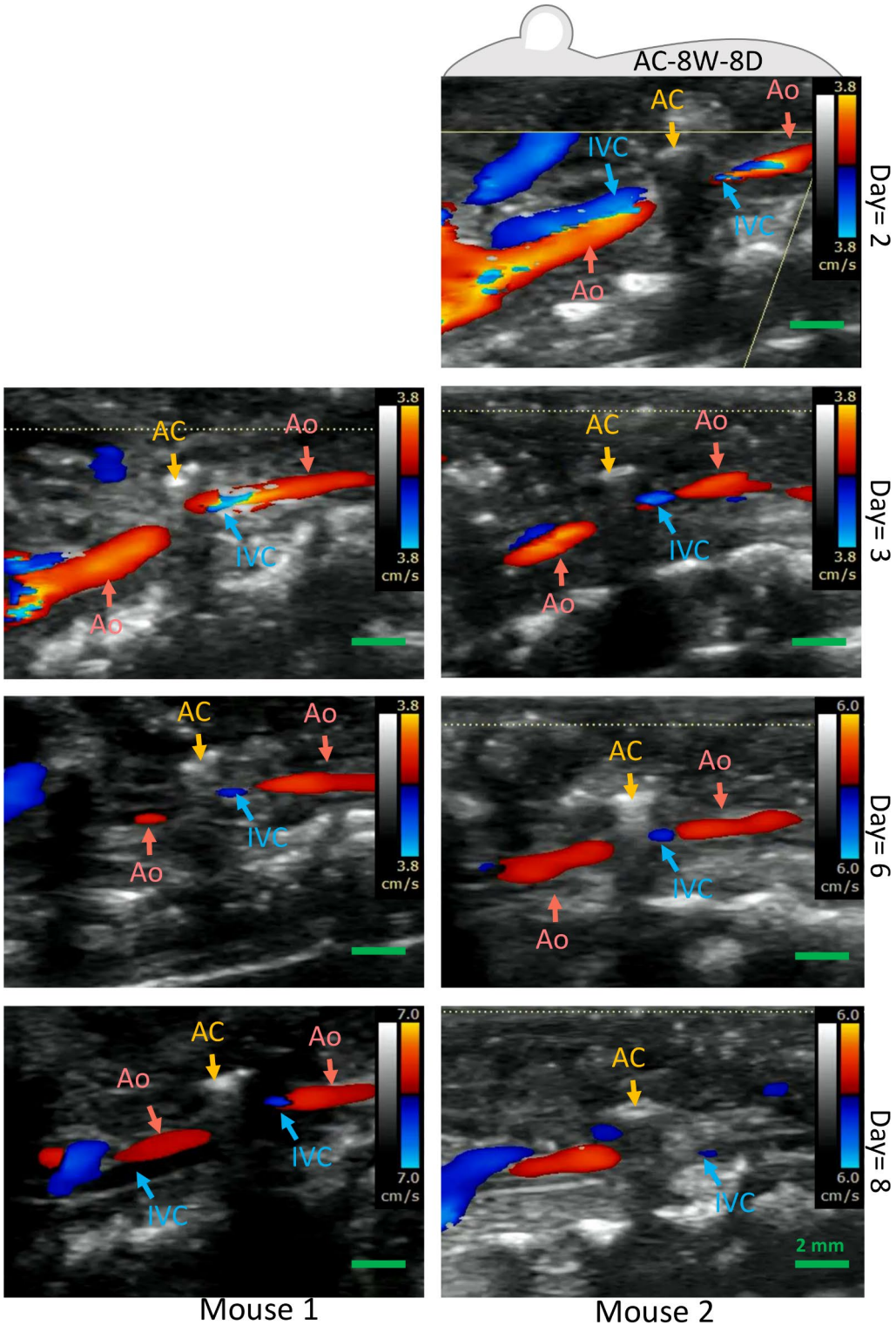

Fig. 6. Effects of AC implantation on IVC blood flow over time. After AC was implanted into the IVC, blood flow in the IVC was observed over time using a color Doppler. Mice 1 and 2 were the same as those in Fig. S6 . The blood vessels will become colored when the measured blood flow velocity exceeds the value indicated on the color bar (mouse 1, days 3 and 6: 3.8 cm/s, day 8: 7.0 cm/s; mouse 2, days 2 and 3: 3.8 cm/s, days 6 and 8: 6.0 cm/s). The orange arrow indicates the position of AC, the light blue arrow indicates the IVC, and the pink arrow indicates the Aorta (Ao). The scale bar (green line) indicates 2 mm. The photos were obtained from the video. AC, ameroid constrictor; IVC, inferior vena cava.

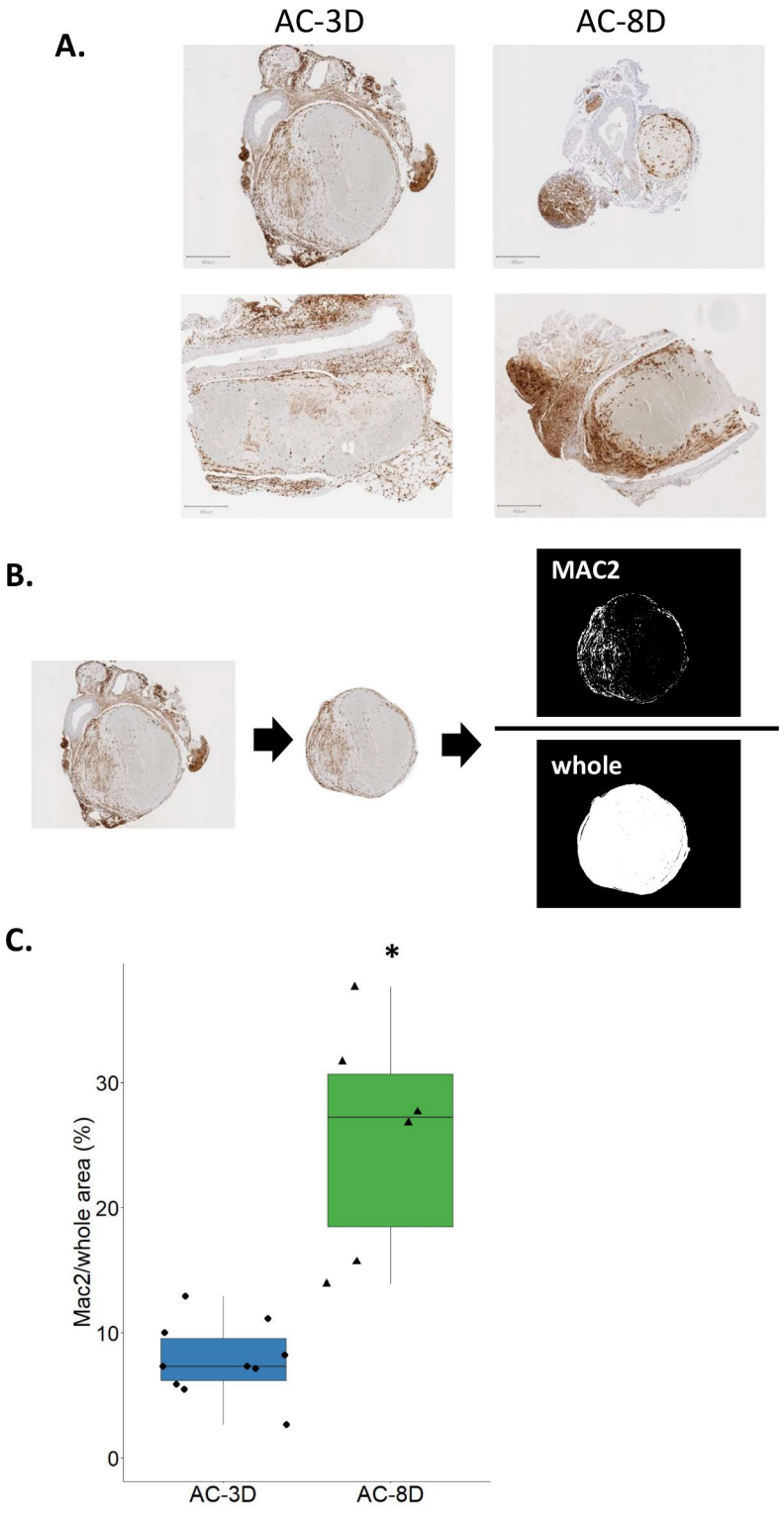

Fig. 7. Macrophage content in thrombus following AC implantation. (A) Representative histological images of tissues removed en bloc with thrombi in IVC subjected to IHC for Mac-2 at 3 (AC-3D) and 8 days (AC-8D) post-AC implantation. Scale bar = 400 μm. (B) Analysis scheme to calculate the percentage of macrophage-containing area on the cross-section of the thrombus. The thrombus image was isolated, and the occupancy rate was calculated as the sum of the Mac-2-positive cell area divided by the whole area of the thrombus section evaluated using *Image J Fiji* . (C) Box and whisker plots comparing occupancy rate in percentage of Mac-2-positive cell infiltration in AC-3D thrombi ($n = 9$) and AC-8D ones ($n = 6$). * $p < 0.05$ (F -test $p = 0.00410$, Welch's t- test $p = 0.00438$). AC, ameroid constrictor; IVC, inferior vena cava; IHC, immunohistochemistry.

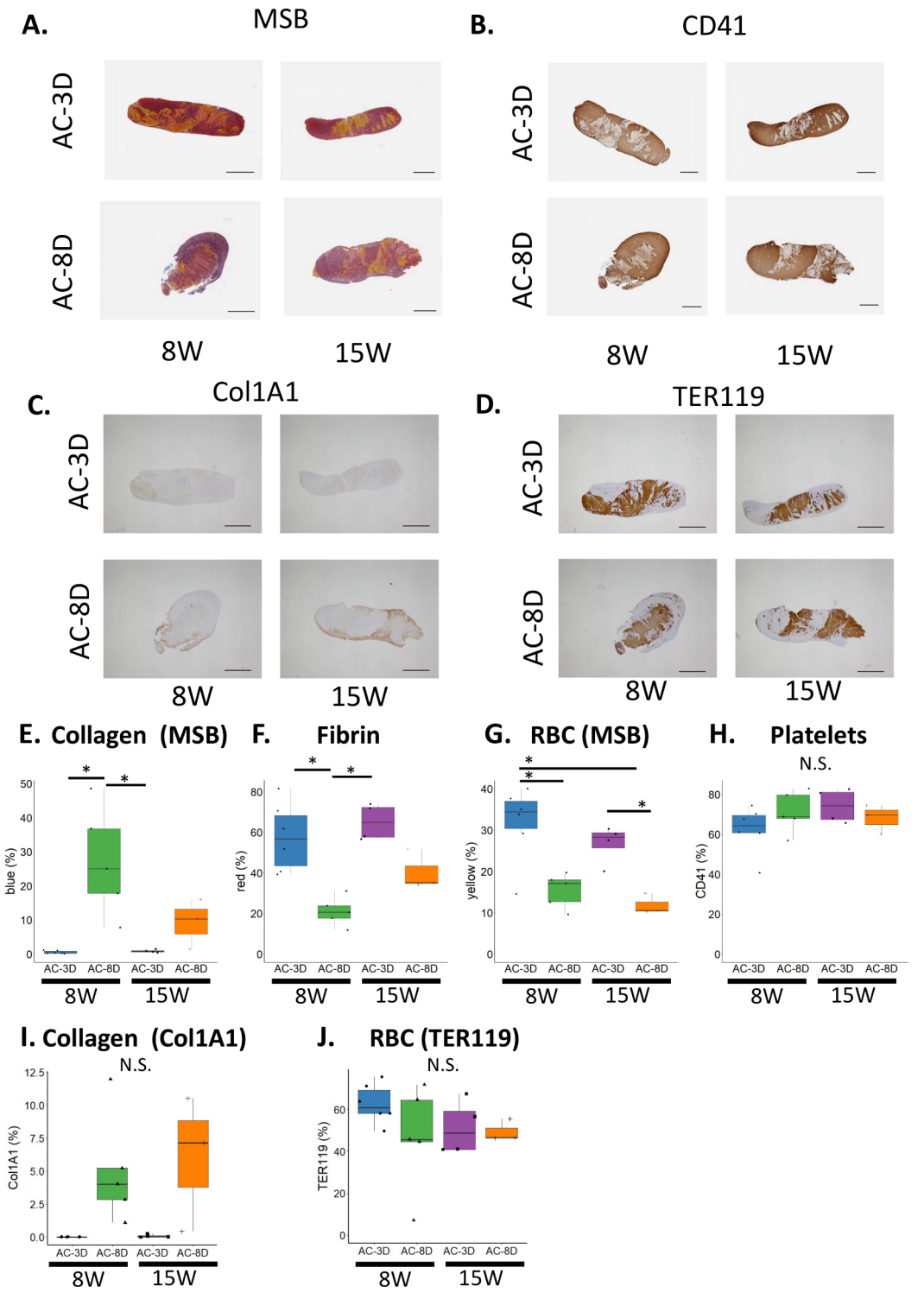

Finally, we compared the composition of collagen, fibrin, and platelets in the thrombus (Fig. S8C–F). Collagen and fibrin levels strongly correlated with thrombi obtained from the AC-8D group (Fig. S8C, F). Extending the duration of AC implantation from 3 to 8 days reduced the amount of fibrin and increased that of collagen in the resulting thrombi. In addition, differences in mouse age did not affect the propensity for thrombus components.

Discussion

This study proposed a novel mouse model of DVT in immunodeficient nude mice using a constricting device made of hygroscopic casein. The IVC-H model reproducibly obtained thrombi with less variation in size while maintaining BF without requiring special skills, compared with conventional DVT models.

In the IVC-H model, we established a procedure for IVC stenosis by simply setting the IVC and aorta together in a ready-made AC device and confirmed BF within the IVC in the model, which is blocked by a thrombus

◀**Fig. 8**. Collagen, fibrin, RBCs, and platelets in thrombi from IVC-H model. (A-D) Representative macroscopic images of thrombi at 3 (AC-3D) and 8 days (AC-8D) in each 8-week-old (8 W) and 15-week-old mice (15 W) following MSB staining (A), after IHC for CD41 labeling platelets (B), after IHC for Col1A1 labeling type I collagen alpha1 chains (C), and after IHC for TER119 labeling red blood cells (D). Scale bar = 1 mm. (A) and (B) were taken with an APERIO CS2 (Leica Biosystems, Tokyo, Japan) and scanned with *QuPath-0.3.2.*(https://qupath.github.io/). (C) and (D) were taken with an ECLIPSE Ni, Digital sight DS-U3, and DS-F12 (Nikon Solutions Co., Ltd., Tokyo, Japan). (E-J) Box and whisker plots comparing the occupying area of each component among thrombi obtained in the AC-8 W-3D, AC-8 W-8D, AC-15W3D, and AC-15 W-8D mice. See methods and the Supplementary Materials for detailed procedures. * $p < 0.05$ (ANOVA and Tukey–Kramer, E: Collagen (MSB), ANOVA $p = 0.002$ and Tukey–Kramer; AC-8 W-3D vs. AC-8 W-8D $p = 0.0028$, AC-8 W-8D vs. AC-15 W-3D $p = 0.00483$, F: Fibrin, ANOVA $p = 5.21 \times 10^{-4}$ and Tukey–Kramer; AC-8 W-3D vs. AC-8 W-8D $p = 0.0029$, AC-8 W-8D vs. AC-15 W-3D $p = 5.22 \times 10^{-4}$, G: RBC (MSB), ANOVA $p = 0.00279$ and Tukey–Kramer; AC-8 W-3D vs. AC-8 W-8D $p = 0.0106$, AC-8 W-3D vs. AC-15 W-8D $p = 0.00687$, AC-15 W-3D vs. AC-15 W-8D $p = 0.0454$, H: Platelets, ANOVA $p = 0.323$, I: Col1A1, ANOVA $p = 0.015$ and Tukey–Kramer; no significant difference, J: TER119, ANOVA $p = 0.397$). AC, ameroid constrictor; ANOVA, analysis of variance; MSB, Martius Scarlet Blue; RBC, red blood cell; IHC, immunohistochemistry.

in the IVC-S model[6]. Additionally, the IVC-S model requires skill and is affected by ligation and spacer type strength[4,5,16]. Therefore, the IVC-L model of simple complete ligation of the IVC is often used; however, it may not accurately reproduce the patient's DVT due to the blockade of BF and the ligation-induced inflammation of the vessel. Consequently, the IVC-H model is the only one that can generate thrombi with high reproducibility while maintaining BF without vascular damage.

Processing of the IVC branches is an important factor for stable thrombogenesis in the IVC-H model, similar to the IVC-L and IVC-S models[7,13,17]. Considering its application in oncology, especially in cancer-associated thromboembolism, we used BALB/c-nu/nu mice in this study. In our study of 52 BALB/c-nu/nu mice, the IVC branches appeared thinner than those reported for the commonly used C57BL/6 mice[13]. Thrombus formation was terminated at the draining sites of the IVC branches that were accidentally left uncauterized in our IVC-H experiments, as previously shown in the IVC-L model with C57BL/6 mice[13]. The processing of the IVC branches based on the anatomical branching patterns in the current study is important for the success and reproducibility of thrombus formation in the IVC-H model, especially in nude mice.

Although DVT is clinically classified based on the time elapsed since symptom onset and is acute within 14 days[18], acute venous thrombosis in the murine IVC-L model was considered as 2–3 days following the ligation procedure owing to the accelerated occurrence of events, probably due to differences in metabolic rates and life spans between mice and humans[6]. In the IVC-L model, a shift in infiltrating blood cells from neutrophils to monocytes, indicating transfer from subacute to the chronic phase of venous thrombi, takes place by day 6[6,19], and collagen becomes the primary component of the thrombus within approximately 8 days post-ligation[20].

In the IVC-H model with AC, monocyte/macrophage infiltration was significantly increased on day 8 compared with day 3 post-AC implantation, and collagen content within the thrombus showed an increasing trend. These results suggest that 3 days post-AC implantation corresponds to the acute phase, whereas 8 days corresponds to the subacute to chronic phase of venous thrombosis. The estimated time of thrombus development in the IVC-H model was similar to that for the IVC-L model[6,20]. In our study, the percentage of red blood cells in AC-8D tissue stained with TER119 antibody was higher than that observed in MSB staining, suggesting that the yellow color of red blood cells was underestimated by MSB staining due to the influence of the blue color of collagen fibers.

Recent advances in mechanical thrombectomy have enabled precise histopathological examination of thrombi, and detailed characteristics of thrombi at different periods since onset have been reported[21–23]. Hendley et al.[22]described the characteristics of a thrombus, dichotomizing it before or at 7 days post-onset, a critical period for direct injection therapy with recombinant tissue plasminogen activator through a catheter. Thrombi retrieved more than 7 days post-onset contain more collagen and fewer RBCs than those retrieved earlier, although the relative amount of platelets remains unchanged[22,23]. Our results on thrombus characteristics in the IVC-H model closely reflected the insight obtained from the human DVT described above; collagen was significantly increased in 8-day thrombi, while the relative number of platelets was unchanged compared with thrombi at 3 days.

We could not fully determine the cause of IVC stenosis in the IVC-H model, which was a limitation of this study. When used for the mouse common carotid artery, the gap of the AC closes after 1 day. The narrowing of the luminal space of the AC progresses over time, sufficient for brain ischemia at 7 days and completes closure at 28 days[14]. The luminal space of the AC in the IVC-H model remained unchanged between the AC at days 3 and 8 and was patent at 28 days post-AC implantation; however, the IVC luminal space was significantly narrowed at 8 days compared with 3 days. Our results indicated that AC implantation narrowed the IVC luminal space.

To explain this observation, we investigated the hypertrophy of the aortic walls, resulting in the compression of IVC because ACs implanted around the common carotid artery of the mouse induce arterial wall hypertrophy[14]. The aortic wall was thickened in the IVC-H models at 3 and 8 days post-AC implantation compared with that in the non-treated controls; however, no significant difference between 3 and 8 days post-AC implantation was observed.

Additionally, there were no significant differences in the aortic lumen area and arterial area between the non-treatment group and the AC implantation groups after 3 and 8 days. These results suggest that AC implantation

does not cause aortic stenosis and that aortic wall hypertrophy is not responsible for the progression of IVC stenosis from 3 to 8 days in the IVC-H model. Holding together an aorta that differs in blood pressure, velocity, and shear stress from the IVC[24] can induce mechanical stress to the IVC, resulting in stenosis progression. Furthermore, the physical expansion of the AC is not the primary cause of vascular occlusion and stenosis[25–28]. Besancon et al. speculated that tissue inflammation and fibrosis caused by the physical expansion of the AC narrows blood vessels[27]. The reduction in the IVC luminal space could be attributed to the increased amount of connective tissue in the AC luminal space. Further studies are warranted to confirm these speculations.

As an additional limitation, the experimental quantification of vessel morphometrics could not be measured in vivo using the ultrasound device in the present study.

In conclusion, we proposed a convenient mouse DVT model in nude mice using the AC, a ready-made constricting device. The IVC-H model successfully generated subacute to chronic thrombi within the IVC with high reproducibility while preserving BF. The model allows us to regulate IVC stenosis by adjusting the amount or concentration of hygroscopic casein used for the AC. This could enable the study of DVT in patients with different conditions. Quantitatively assessing BF through the pulse waveform is essential for a deeper understanding of thrombus formation in the IVC-H model. This highly reproducible thrombus-generation animal model maintains BF in the IVC and allows for the xenografting of human cancer cells as developed in immunocompromised nude mice. By engrafting patient-derived tumors or established human cancer cell lines, the model can partly reproduce the cancer-bearing condition of patients and facilitates research on CAT. The maintained BF in this model broadened its potential will use to study anticancer drug-induced DVT or anticoagulant development, contributing to the field of oncology and cardiovascular disease. In addition, the blood thrombus composition obtained from this model mirrored that in patients with venous thromboembolism, highlighting the applicability of this animal model.

Methods

Experimental animals

All animal studies followed the Animal Research: Reporting of In Vivo Experiments guidelines and were approved by the Institutional Animal Experiment Committee of Kanagawa Cancer Center, Japan (Approval No. 04 – 03). All methods were performed following the relevant guidelines and regulations (Figure S1).

Female BALB nude (BALB/c-nu/nu) mice aged 7–20 weeks were purchased from Charles River Laboratories Japan (Yokohama, Japan). Mice were intraperitoneally administered a mixture of medetomidine, midazolam, and butorphanol (Me: 0.3 mg/kg, Mi: 4.0 mg/kg, and Bu: 5.0 mg/kg) as anesthesia for each surgery. After each treatment, the mice were isolated individually in cages and warmed overnight using warmers placed under the cages. All mice underwent cardiac blood collection while inhaling isoflurane and were immediately euthanized by cervical dislocation. In this study, n refers to the number of animals or samples obtained from one animal.

IVC-H model

Midline laparotomy followed by dislocation of the intestine to the left side exposed the IVC (Fig. 1A–D). The right ovarian vein was first identified and cauterized, and the IVC and aorta were separated from the surrounding tissues (Fig. 1D a); the cauterizing branches of the IVC were identified during this procedure. The dimensions of AC (MC-1.00-Ti, Research Instruments NW Inc., Lebanon, OR, USA) were lumen, 1 mm in diameter; gap, 0.6 mm; cuff (metal ring), 3.25 mm in diameter of outer circumference; length, 1.25 mm. Saline was added to the field of the procedure, followed by the immediate removal of excess saline to achieve smooth slipping of the AC. A cotton swab was used to pull the IVC and aorta to the left (Fig. 1D b), the AC was inserted through the gap, and the AC was pulled slightly to the right to pinch the aorta in the gap (Fig. 1D c). Then, by gently moving the AC up and down with tweezers, the IVC and aorta were set into the AC cavity by gently pushing with a cotton swab from the other side (Fig. 1D d, e). Finally, the AC was rotated such that the gap faced upward (Fig. 1D f), and the IVC and aorta were completely in the lumen (Fig. 1D g). Methods for the conventional IVC-L model are provided in the Supplementary Materials.

Eight- or 15-week-old BALB/c-nu/nu mice were subjected to the IVC-H model and euthanized for examination 3 or 8 days post-AC implantation. The experimental groups were designated as AC-8 W-3D ($n=12$), AC-8 W-8D ($n=12$), AC-15 W-3D ($n=4$), and AC-15 W-8D ($n=4$). The AC status was evaluated 28 days post-AC implantation using 10-week-old mice.

Histological examinations and ultrasonographic live imaging

Mouse tissues, including the IVC, aorta, and thrombus, were removed *en bloc*, followed by separation of the thrombus, and fixed in 10% formalin. The weight and length of the thrombus were measured before fixation.

Specimens were then embedded in paraffin and subjected to hematoxylin-eosin (HE) staining (IVC and aorta) or MSB staining and IHC for CD31, smooth muscle actin, CD41, and Mac-2 Ab (for thrombus) analysis. Metrological analysis of the IVC and aorta was conducted using *ImageJ Fiji* software (National Institutes of Health, Bethesda, MD, USA).

In two IVC-H model mice, live imaging of BF in the IVC and aorta was performed with ultrasonography every day from the AC implantation to day 8. Precise methods and information for histological examinations and ultrasonography are provided in the Supplementary Materials.

Statistics

Continuous variables (weight and length of thrombi) are presented as the mean ± standard deviation (SD; 95% confidence intervals). The SD for each value was compared using the *F*-test to evaluate the variability between the two experimental groups. The Student's *t*-test was used for $p > 0.05$ in the *F*-test, while the Welch's *t*-test was performed for $p < 0.05$. All tests were two-tailed. The Tukey–Kramer or Dunnett method was applied to compare

multiple experimental groups after a one-way analysis of variance. *Microsoft Excel* (Microsoft Corporation, Redmond, WA, USA) was used for all analyses except for Dunnett's method, which was performed using the *R package EZR* (R Core Team, Vienna, Austria).

Data availability

Data supporting the findings of this study are available within the article and its additional files.

Received: 14 June 2024; Accepted: 23 December 2024
Published online: 06 January 2025

References

1. Khorana, A. A. et al. Cancer-associated venous thromboembolism. *Nat. Rev. Dis. Prim.* **8**, 1–18 (2022).
2. Bertoletti, L. et al. Cancer-associated thrombosis: Trends in clinical features, treatment, and outcomes from 2001 to 2020. *JACC CardioOncol*. **5**, 758 (2023).
3. Wrobleski, S. K., Farris, D. M., Diaz, J. A., Myers, D. D. & Wakefield, T. W. Mouse complete stasis model of inferior vena cava thrombosis. *J. Vis. Exp.* **52**, 2738 (2011).
4. Brill, A. et al. Von Willebrand factor-mediated platelet adhesion is critical for deep vein thrombosis in mouse models. *Blood* **117**, 1400–1407 (2011).
5. Wang, J. G. et al. Tumor-derived tissue factor activates coagulation and enhances thrombosis in a mouse xenograft model of human pancreatic cancer. *Blood* **119**, 5543–5552 (2012).
6. Diaz, J. A. et al. Critical review of mouse models of venous thrombosis. *Arterioscler. Thromb. Vasc Biol.* **32**, 556–562 (2012).
7. Diaz, J. A. et al. Choosing a mouse model of venous thrombosis: a consensus assessment of utility and application. *Arterioscler. Thromb. Vasc Biol.* **39**, 311–318 (2019).
8. Mackman, N. Mouse models of venous thrombosis are not equal. *Blood* **127**, 2510–2511 (2016).
9. Geddings, J. et al. Strengths and weaknesses of a new mouse model of thrombosis induced by inferior vena cava stenosis: communication from the SSC of the ISTH. *J. Thromb. Haemost.* **12**, 571 (2014).
10. Mackman, N. New insights into the mechanisms of venous thrombosis. *J. Clin. Invest.* **122**, 2331–2336 (2012).
11. Hisada, Y., Ay, C., Auriemma, A. C., Cooley, B. C. & Mackman, N. Human pancreatic tumors grown in mice release tissue factor-positive microvesicles that increase venous clot size. *J. Thromb. Haemost.* **15**, 2208–2217 (2017).
12. Sasano, T. et al. Role of tissue-factor bearing extracellular vesicles released from ovarian cancer cells in platelet aggregation in vitro and venous thrombosis in mice. *Thromb. Updat.* **2**, 100020 (2021).
13. Diaz, J. A., Farris, D. M., Wrobleski, S. K., Myers, D. D. & Wakefield, T. W. Inferior vena cava branch variations in C57BL/6 mice have an impact on thrombus size in an IVC ligation (stasis) model. *J. Thromb. Haemost*. **13**, 660–664 (2015).
14. Hattori, Y. et al. Gradual carotid artery stenosis in mice closely replicates hypoperfusive vascular dementia in humans. *J. Am. Heart Assoc.* **5**, 1–12 (2016).
15. Krishna, S. M. et al. Development of a two-stage limb ischemia model to better simulate human peripheral artery disease. *Sci. Rep.* **10**, 1–16 (2020).
16. von Brühl, M. L. et al. Monocytes, neutrophils, and platelets cooperate to initiate and propagate venous thrombosis in mice in vivo. *J. Exp. Med.* **209**, 819–835 (2012).
17. Brandt, M. et al. Deep vein thrombus formation induced by flow reduction in mice is determined by venous side branches. *Clin. Hemorheol Microcirc*. **56**, 145–152 (2014).
18. Vedantham, S. et al. Quality improvement guidelines for the treatment of lower-extremity deep vein thrombosis with use of endovascular thrombus removal. *J. Vasc Interv Radiol.* **25**, 1317–1325 (2014).
19. Ten Cate-Hoek, A. J., Henke, P. K. & Wakefield, T. W. The post thrombotic syndrome: ignore it and it will come back to bite you. *Blood Rev.* **30**, 131–137 (2016).
20. Nicklas, J. M., Gordon, A. E. & Henke, P. K. Resolution of deep venous thrombosis: proposed immune paradigms. *Int. J. Mol. Sci.* **21**, 2080 (2020).
21. Hendley, S. A. et al. Assessment of histological characteristics, imaging markers, and rt-PA susceptibility of ex vivo venous thrombi. *Sci. Rep.* **11**, 22805 (2021).
22. Horne, M. K. & Chang, R. Thrombolytic therapy for deep venous thrombosis? *JAMA* **282**, 2164–2166 (1999).
23. Silver, M. J. et al. Histopathologic analysis of extracted thrombi from deep venous thrombosis and pulmonary embolism: mechanisms and timing. *Catheter Cardiovasc. Interv*. **97**, 1422–1429 (2021).
24. Kudze, T. et al. Altered hemodynamics during arteriovenous fistula remodeling leads to reduced fistula patency in female mice. *JVS Vasc Sci.* **1**, 42–56 (2020).
25. Adin, C.A., Acvs, D., Gregory, C.R et al. Effect of Petrolatum Coating on the Rate of Occlusion of Ameroid Constrictors inthe Peritoneal Cavity. https://doi.org/10.1111/j.1532-950x.2004.04001.x, (2004).
26. Youmans, K.R., Hunt, G.B. Experimental Evaluation of Four Methods of Progressive Venous Attenuation in Dogs.https://doi.org/10.1053/jvet.1999.0038, **28**(1), 38–47 (1999).
27. Besancon, M.F, Kyles, A.E., Griffey, S.M., Gregory, C.R. Evaluation of the characteristics of venous occlusion after placementof an ameroid constrictor in dogs. *Vet Surg.* **33**(6), 597–605, https://doi.org/10.1111/J.1532-950X.2004.04082.X, (2014).
28. Hunt, G.B. Evaluation of in vivo behavior of ameroid ringconstrictors in dogs with congenital extrahepatic portosystemic shunts using computed tomography. *Vet Surg.*, *43*(7), 834–842, https://doi.org/10.1111/J.1532-950X.2014.12196.X, (2014).

Acknowledgements

We would like to thank Kumiko Ohrui (Kanagawa Cancer Center Research Institute), Shizuka En, and Yuya Suzuki (LABOTECH Co., Ltd.) for their help with the animal experiments. We thank Editage (www.editage.jp) for English language editing.

Author contributions

H.T. and Y.O. performed animal experiments. H.T. and M.U. performed ultrasound imaging. Y.N. and M.Y. performed histological staining. Y.T. and Y.N. advised on ultrasound imaging. H.T. performed all data processing and statistical analysis. H.T. and Y.M. designed the experiments. H.T. wrote the manuscript, S.K., and E.M. advised the manuscript, and S.S., and Y.M. edited the manuscript.

Funding
This research received no specific grant from funding agencies in the public, commercial, or not-for-profit sectors.

Declarations

Competing interests
The authors declare no competing interests.

Ethics approval
All animal studies followed the ARRIVE guidelines and were approved by the Institutional Animal Experiment Committee of Kanagawa Cancer Center, Japan (Approval No. 04 – 03).

Additional information
Supplementary Information The online version contains supplementary material available at https://doi.org/10.1038/s41598-024-84443-8.

Correspondence and requests for materials should be addressed to Y.M.

Reprints and permissions information is available at www.nature.com/reprints.

Publisher's note Springer Nature remains neutral with regard to jurisdictional claims in published maps and institutional affiliations.